Evaporation of a Heated Falling Liquid Film into a Laminar Gas Stream

Y. L. Tsay
T. F. Lin
Department of Mechanical Engineering,
National Chiao Tung University,
Hsinchu, Taiwan, Republic of China

■ Heat and mass transfer characteristics for a falling liquid film evaporating into a gas stream were investigated. The liquid water film falls along a vertical plate subjected to a uniform heat flux. In the numerical analysis the respective governing equations for the liquid film and gas stream were solved together. An experimental system was also set up to measure the heat transfer coefficient along the wetted wall for various thermal and flow conditions. The measured data are in good agreement with the numerical predictions. It is observed that the latent heat transport connected with the vaporization of the liquid film plays an important role in the transfer processes. A correlation of the Nusselt number for heat transfer from the wetted wall to the liquid film is proposed.

Keywords: *heated liquid film, gas stream, evaporation, latent heat transfer*

INTRODUCTION

Heat transfer augmentation through latent energy transport during the vaporization of a liquid film, or evaporative cooling, is often encountered in the cooling of microelectronic equipment, the protection of system components from high-temperature gas streams in supersonically flying vehicles and in combustion chambers, the design of cooling towers, and in many other applications. The purpose of this study is to investigate the evaporative cooling process by performing a detailed analysis of heat and mass transfer in a laminar gas stream flowing over a heated falling liquid film, complemented with experimental measurement.

Chun and Seban [1] and Seban and Faghri [2] experimentally and theoretically investigated the evaporation from a liquid water film into a pure water vapor. In their theoretical studies they focused on the transport processes in the liquid film. In view of the complexity of the coupling between the momentum, heat, and mass transfer in the gas flow and the momentum and heat transfer in the liquid film through their common interface, other early studies primarily focused their attention on the heat and mass transfer in the air stream by assuming the liquid film to be extremely thin. Under this assumption, transport in the film can be replaced by the appropriate boundary conditions for the gas flow. This type of analysis was carried out for the buoyancy-induced heat and mass transfer over flat plates with different inclinations [3–7] and inside a circular pipe [8]. A similar analysis was carried out by Chandra and Savery [9, 10] for an upward forced airflow over a free-falling isopropyl alcohol film by the integral method. In their theoretical work the measured temperature and concentration distributions along the gas/liquid interface were used to specify the nonhomogeneous boundary conditions required for solving the energy and species diffusion equations for the air–vapor flow. In addition, laminar and turbulent forced convection boundary layer flows of gas over a vaporizing liquid film on a flat plate were numerically investigated by Schroppel and Thiele [11] with the same assumption. Similar studies were conducted by Chow and Chung [12, 13] for laminar and turbulent airflow of various humidities and superheated stream over a liquid water film. The evaporation rates of water were measured by Haji and Chow [14], and the measured data agreed well with the predicted values [13] if the heat loss from the water pan is accounted for.

Analyses including transport processes in the gas flow and liquid film were conducted for turbulent gas flow over a concurrent liquid flow by Shembharkar and Pai [15] and Baumann and Thiele [16]. However, in these studies the temperature distributions across the film were assumed to be linear.

The preceding review reveals that interactions between a falling liquid film and gas stream have not been properly treated in the literature. The main objective of this study is to experimentally and theoretically explore the detailed heat and mass transfer characteristics for a heated falling liquid film evaporating into a gas stream. The geometry of the system to be investigated is schematically shown in Fig. 1. A vertical plate is wetted by a thin liquid water film

Liquid water   Gas stream
$T_{L,in}, \dot{m}_{L,in}$ $T_{G,\infty}, U_{G,\infty}, W_{v,\infty}$
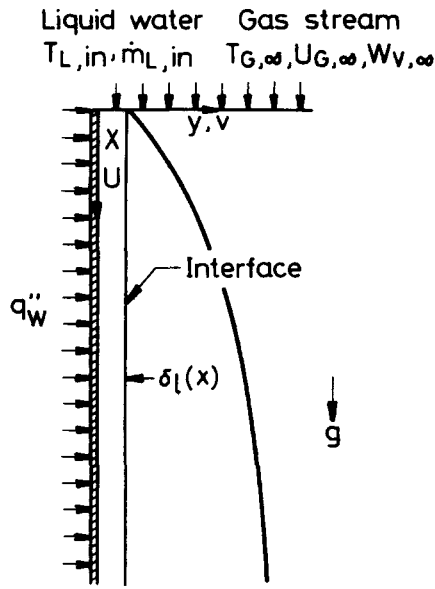

Figure 1. Schematic diagram of the physical system.

fed at a constant temperature $T_{L,in}$ and constant flow rate $\dot{m}_{L,in}$. The falling liquid film is exposed to a downward forced gas stream with a constant free-stream velocity $u_{G,\infty}$, free-stream temperature $T_{G,\infty}$, and water vapor concentration $W_{v,\infty}$. The plate wall is subjected to a uniform wall heat flux q''_w. With the introduction of a liquid film on the heated surface, great enhancement in the heat transfer rate can be obtained because of the presence of combined heat and mass transfer. Thus, this cooling method has the capability to transfer a large quantity of heat while maintaining the heat transfer surface at a low temperature. In this study we performed a detailed numerical analysis by simultaneously solving the conservation equations for various transport processes in the liquid film and gas stream, with the interface-matching conditions properly treated. Attention was particularly focused on the latent heat transfer associated with the film vaporization and the variations in the heat transfer coefficient for heat transfer from the wetted wall to the liquid film. To complement the numerical analysis, an experimental system was established to measure the temperature distributions along the wetted wall for various thermal and flow conditions.

ANALYSIS

As the liquid film falls along a heated plate, part of the liquid water evaporates into the gas stream. Thus, heat and mass transfer occur simultaneously at the interface. The interface heat and mass transfer is apparently determined by the coupled transport processes in the liquid film and gas stream. The transport processes in the liquid film are affected by the interface shearing effect and vaporization along the interface, whereas the forced gas stream is influenced by the evaporating vapor, the interface shearing effect, and the combined buoyancy effects of thermal and mass diffusion.

Basic Equations for the Liquid Film

Since only low liquid flow rates are considered here, the inertia terms in the momentum equation are small compared with the body force term and can be neglected. Furthermore, for the thin liquid film the longitudinal gradients of velocity and temperature are much smaller than those in the transverse direction. With these simplifications, the steady laminar momentum and heat transfer in the liquid film can be described by the following equations.

X-momentum equation:

$$0 = \frac{\partial}{\partial y}\left(\mu_L \frac{\partial u_L}{\partial y} \right) + \rho_L g. \tag{1}$$

Energy equation:

$$\rho_L C_{p_L} u_L \frac{\partial T_L}{\partial x} = \frac{\partial}{\partial y}\left(\lambda_L \frac{\partial T_L}{\partial y} \right). \tag{2}$$

Basic Equations for Gas Flow

Steady laminar mixed convection heat and mass transfer in the gas flow can be explored, with the usual boundary layer approximations, by the following basic equations.

Continuity equation:

$$\frac{\partial}{\partial x}(\rho_G u_G) + \frac{\partial}{\partial y}(\rho_G v_G) = 0. \tag{3}$$

X-momentum equation:

$$\rho_G\left(u_G \frac{\partial u_G}{\partial x} + v_G \frac{\partial u_G}{\partial y} \right) = \frac{\partial}{\partial y}\left(u_G \frac{\partial u_G}{\partial y} \right) + (\rho_G - \rho_\infty)g. \tag{4}$$

Energy Equation:

$$\rho_G C_{p_G}\left(u_G \frac{\partial T_G}{\partial x} + v_G \frac{\partial T_G}{\partial y} \right)$$
$$= \frac{\partial}{\partial y}\left(\lambda_G \frac{\partial T_G}{\partial x} \right) + \rho_G D(C_{pv} - C_{pa})\frac{\partial T_G}{\partial y} \frac{\partial W_v}{\partial y}. \tag{5}$$

Species diffusion equation of water vapor:

$$\rho_G\left(u_G \frac{\partial W_v}{\partial x} + v_G \frac{\partial W_v}{\partial y} \right) = \frac{\partial}{\partial y}\left(\rho_G D \frac{\partial W_v}{\partial y} \right). \tag{6}$$

Boundary and Interface Conditions

The boundary conditions are
At $x = 0$,

$$T_L = T_{L,in}, \quad T_G = T_{G,\infty}, \quad u_G = u_{G,\infty}, \tag{7a}$$
$$v_G = 0, \quad W_v = W_{v,\infty}.$$

At $y = 0$,

$$u_L = 0, \quad \frac{\partial T_L}{\partial y} = -\frac{q''_w}{\lambda_L}. \tag{7b}$$

At $y \to \infty$,

$$u_G = u_{G,\infty}, \quad T_G = T_{G,\infty}, \quad W_v = W_{v,\infty}. \tag{7c}$$

The interface-matching conditions specified at $y = \delta_L(x)$ are the following.

1. The continuity of velocity, temperature, and shear stress is expressed as

$$u_{L,i} = u_{G,i}, \qquad T_{L,i} = T_{G,i},$$

$$\left(\mu_L \frac{\partial u_L}{\partial y}\right)_{L,i} = \left(\mu_G \frac{\partial u_G}{\partial y}\right)_{G,i}. \qquad (8)$$

2. The transverse velocity of the air–vapor mixture, deduced by assuming that the interface is semipermeable —that is, the solubility of air in liquid water is negligibly small and the air velocity in the y direction is zero at the interface, is

$$v_{G,i} = -\left(\frac{D}{1 - W_{v,i}}\right)\left(\frac{\partial W_v}{\partial y}\right)_{G,i}. \qquad (9)$$

3. Assuming that the interface is at thermodynamic equilibrium and the air–water vapor mixture is an ideal gas mixture, the mass fraction of the water vapor can be calculated as [8]

$$W_{v,i} = \frac{M_v P_{v,i}}{M_a(P_\infty - P_{v,i}) + M_v P_{v,i}}, \qquad (10)$$

where $P_{v,i}$ is the saturation pressure of water at the interface temperature.

4. The energy balance at the interface is

$$-\lambda_L\left(\frac{\partial T_L}{\partial y}\right)_{L,i} = -\left(\lambda_G \frac{T_G}{\partial y}\right)_{G,i} + m''_{v,i} h_{LG}, \qquad (11)$$

where the vaporizing flux of the water vapor is calculated by using the equation

$$m''_{v,i} = -\left(\frac{\rho_{G,i} D}{1 - W_{v,i}}\right)\left(\frac{\partial W_v}{\partial y}\right)_{G,i}. \qquad (12)$$

Equation (11) indicates that energy exchange between the gas stream and liquid film depends on two related factors: the interface temperature gradient at the gas side, resulting in sensible heat transfer, and the rate of mass transfer, resulting in latent heat transfer. The total heat transfer from the interface into the gas stream can then be expressed as

$$q''_i = q''_{s,i} + q''_{e,i}$$

$$= -\left(\lambda_G \frac{\partial T_G}{\partial y}\right)_{G,i} - \left(\frac{\rho_{G,i} D h_{L,G}}{1 - W_{v,i}}\right)\left(\frac{\partial W_v}{\partial y}\right)_{G,i}. \qquad (13)$$

The coefficient for heat transfer from the wetted wall to the liquid film, which is important in many engineering applications, is evaluated as

$$h_L = \frac{q''_w}{T_w - T_{L,in}}. \qquad (14)$$

Then the local Nusselt number for heat transfer from the wetted wall to the liquid film, based on the characteristic length $(\nu_L^2/g)^{1/3}$ [1], is defined as

$$Nu_L = \frac{h_L(\nu_L^2/g)^{1/3}}{\lambda_L} = \frac{q''_w(\nu_L^2/g)^{1/3}}{\lambda_L(T_w - T_{L,in})}. \qquad (15)$$

It is noted that in the above formulation the thermophysical properties of the liquid film and gas mixture are considered to be variables depending on temperature and mixture composition. They are calculated from the pure component data by means of the mixing rules [17]. The pure component data are available in [18, 19]. Additionally, we note that the wave motion of the liquid/gas interface and the entrainment of the liquid in the form of droplets into the gas stream may be important when the relative motion of the gas flow against the liquid film is large. These processes are rather complex and are neglected in the present study because of a lack of adequate information.

SOLUTION METHOD

Since the flows governed by Eqs. (1)–(6) are parabolic in x, the finite-difference solution for these equations can be marched in the downstream direction. A fully implicit numerical scheme, in which the longitudinal convection terms are approximated by the upstream difference and the transverse convection and diffusion terms by the central difference, is employed to transform the governing equations into finite-difference equations. Each system of the finite-difference equations forms a tridiagonal matrix equation that can be efficiently solved by the Thomas algorithm [20]. For a given flow and thermal condition a brief outline of the solution procedures is described as follows.

1. For a given longitudinal location x_j, assume a film thickness $\delta_{L,j}$.
2. Solve the finite-difference forms of Eqs. (1) and (4) simultaneously for u_L and u_G.
3. Numerically integrate Eq. (3) to find v_G.
4. Solve the finite-difference forms of Eqs. (2) and (5) together for T_L and T_G.
5. Solve the finite-difference form of Eq. (6) for W_v.
6. Check whether the relative error between two consecutive iterations $n - 1$ and n is small enough, that is, $|\varphi^n - \varphi^{n-1}|/|\varphi^n|_{max} < 10^{-3}$ for all nodal points, where φ represents variables u_G, u_L, T_G, T_L, or W_v. If not, repeat steps 2–6.
7. Check the mass conservation of the liquid water film by examining the satisfaction of the inequality

$$\left|\frac{(\dot{m}_{L,j-1} - \dot{m}_{L,j}) - (m''_{vi,j}\Delta x_j)}{\dot{m}_{L,j-1} - \dot{m}_{L,j}}\right| < 10^{-4}, \qquad (16)$$

where

$$\dot{m}_{L,j} = \int_0^{\delta_{L,j}} \rho_L u_L \, dy. \qquad (17)$$

8. If Eq. (16) is not satisfied, assume a different film thickness and repeat steps 2–7 for the current axial location. If it is satisfied, proceed to the next axial location and apply steps 1–7.

To account for the change in the liquid film thickness $\delta_L(x)$ in the flow direction due to film vaporization, the finite-difference computational grid used must comply with the variation of the computation domain with x. This was accomplished by first locating the interface at a given x location and then dividing the film and gas regions in the

y direction into n_L and n_G points, respectively. Thus the interface position was rigorously traced. This adjustment of the grid in the y direction necessitates numerical interpolation when evaluating the convection terms. To further account for the drastic variations of the velocity, temperature, and concentration in the regions near the leading edge and the interface, a nonuniform grid was chosen. The computation domain was taken to be 0.5 m in the x direction and 0.025 m in the y direction for various cases. The nonuniformity of the grid is described here in detail. $\Delta x_1 = 1.45 \times 10^{-3}$ m and $\Delta x_j = 1.005 \times \Delta x_{j-1}$; in the film, $\Delta y_1 = 9.35 \times 10^{-5}$–$15.6 \times 10^{-6}$ m close to the plate and $\Delta y_k = 0.95 \times \Delta y_{k-1}$; in the gas flow, $\Delta y_1 = 7.3 \times 10^{-5}$ m near the interface and $\Delta y_k = 1.005 \times \Delta y_{k-1}$.

During the program test, several grid sizes were employed to check the grid independence. It is noted in the separate computations that the differences in results obtained by using the 201×221 and 301×331 grids are always less than 2%. Accordingly, the computations using the 201×221 grid are considered to be sufficiently accurate to describe the transfer characteristics in the present problem. To further check the adequacy of the numerical scheme employed for the present study, results for the limiting case of laminar mixed convection heat transfer along a vertical plate with opposing buoyancy force are obtained. Excellent agreement between the present predictions and those of Szewczyk [21] was noted. This further supports the employment of the present numerical scheme.

EXPERIMENTAL APPARATUS

Depicted in Fig. 2 is the schematic arrangement of the experimental setup. This experimental apparatus is designed particularly for investigating the evaporation of liquid film into a mixed convection gas stream. As shown in Fig. 2, liquid water falls along a vertical plate from a liquid distributor and is collected as it leaves the plate. The liquid in the collector is then pumped to a reservoir in which it is heated by a preheater. The air passes through a convergent nozzle, then a honeycomb, and finally into the test section.

Basically, the experimental apparatus consists of five parts: wind tunnel, liquid delivery system, heating facilities, and the measuring probes and data acquisition system. Descriptions of these facilities follow.

Wind Tunnel

As shown in Fig. 2, the wind tunnel is placed vertically above the test section in the buoyancy-opposing flow condition. The tunnel has a smooth converging nozzle with a contraction ratio of 10 : 1, a vertical straight test section, and a smooth buffer section. A honeycomb is installed in the exit section of the converging nozzle to produce uniform velocity and to reduce turbulence at the inlet of the test section. The converging nozzle is constructed with 1.5-mm-thick SS-304 steel plates with adequate frames and supports to provide a rigid structure. At the end of the buffer section, a variable-speed blower is used to pass air through the test section. The test section
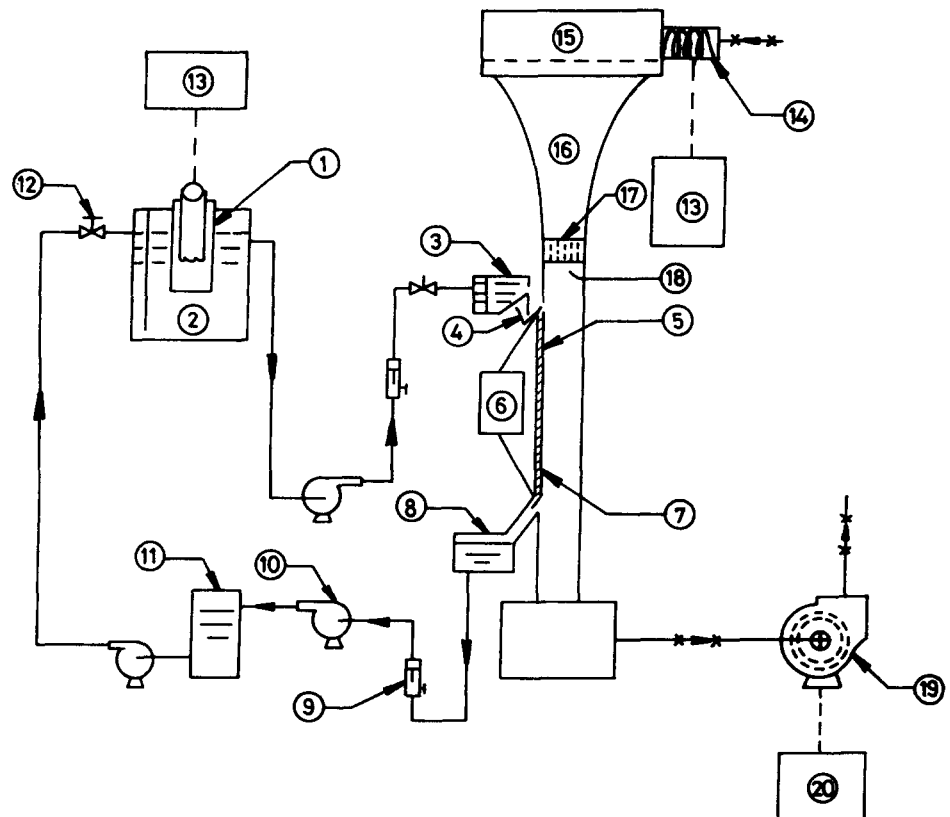

Figure 2. Schematic diagram of experimental apparatus. 1, Liquid preheater; 2, liquid reservoir; 3, feed tank; 4, liquid distributor; 5, steel plate; 6, power supply; 7, insulated plate; 8, liquid collector; 9, liquid flowmeter; 10, pump; 11, liquid collector; 12, valve; 13, temperature controller and power supply; 14, air preheater; 15, air tank; 16, nozzle; 17, honeycomb; 18, Pitot tube; 19, blower; 20, motor and frequency regulator.

is a rectangular channel 220 × 160 mm in cross section and 500 mm long, with three sides made of acrylic plates and another made of stainless steel plate. The stainless steel plate is 50 cm long, 21 cm wide, and 1 mm thick. Fourteen calibrated copper-constantan thermocouples are glued onto the back surface of the plate to measure its temperature. To prevent heat loss from the plate to the surroundings, the plate is insulated with plastic and wood.

At the buffer end, a variable-speed blower provides air with velocities up to 10 m/s through the vertical channel in the test section. The speed of the blower is controlled by an ac motor speed controller with an output frequency of 0–60 Hz and full load current of 4 A. To reduce the influence of vibration from the blower, a flexible connector made of cloth is employed to connect the blower and the buffer end.

Liquid Delivery System

The closed-loop liquid delivery system consists of a liquid reservoir, a feed tank, a liquid distributor, a steel plate, two liquid collectors, and three pumps, as shown in Fig. 2. The liquid water stored in the reservoir is pumped into the feed tank and enters the liquid distributor. In the distributor the liquid becomes calm and is then distributed along the width of the entrance opening between the steel plate and the acrylic plate. The liquid then moves through the entrance opening and falls along the vertical steel plate. Upon leaving the steel plate, the liquid is collected in a collector and is then pumped back to the reservoir, where it is heated by a liquid preheater.

Heating Facilities

In the present experiment, heating facilities are required to control the air temperature at the channel inlet, the liquid temperature just before the liquid moves onto the plate, and the electric power input to the heated steel plate.

Liquid Preheater To accurately control the liquid temperature in the reservoir, an automatic feedback heating system comprising a very sensitive Pt rod, a temperature controller, and an ac power supply is used. As shown in Fig. 2, the liquid in the reservoir is heated by the water stored in a small tank, which is heated by two resistance coils. The electric current passed through the coils is supplied by a 6-kW ac power supply.

Air Preheater As shown in Fig. 2, before the air enters the air tank it is sucked into an air preheater. The preheater system consists of resistance coils, a 6-kW ac power supply, a very sensitive Pt rod, and a temperature controller. Thus the air temperature at the inlet of the test section can be accurately controlled.

Plate Heating Facilities Two copper conductors are screwed to the top and bottom of the stainless steel plate (50 cm long, 21 cm wide, and 1 mm thick). Direct electric current, generated by a 10-kW dc power supply, is passed through the steel plate to provide the required heating.

The electric power input to the heated steel plate is determined from the measured voltage drop across the plate and the current passing through it,

$$\dot{Q}_{tot} = IV = I^2 \frac{\rho_e l}{\delta_w z} \qquad (18)$$

where I and V are electric current and voltage, and ρ_e is the electrical resistivity of the plate. To accurately measure the electric current, a shunt is arranged between the cables.

Measuring Probes and Data Acquisition System

In the experiments, temperature, liquid, and gas flow rates and the power applied to the steel plate are measured.

Temperature Measurements and Data Acquisition System
Copper-constantan (T-type) thermocouples are used to measure the temperatures. Prior to installation, the thermocouples are calibrated by a LAUDA compact low-temperature thermostat (Type RKS20-D) with a YEW digital thermometer (Type 2575). The overall accuracy of the thermocouples is believed to be well within 0.15°C.

To measure the temperature distribution of the steel plate, 10 thermocouples are installed on the back surface of the plate along the longitudinal centerline and spaced 5 cm apart. To assess the uniformity of the liquid film along the plate, three thermocouples are installed spanwise across the plate at two longitudinal locations. In each experimental run, the measured wall temperature differences among three locations at the same X are controlled to be less 0.2°C. Therefore, we have confidence that spanwise uniformity of the liquid film across the plate is obtained.

The front surface temperature of the steel plate at the measuring locations is estimated from the measured back surface temperature according to the steady-state heat conduction solution for a slab. The slab is assumed to be subjected to uniform internal heat generation and a prescribed heat flux at the back surface, accounting for the heat loss through the insulator to the ambient. The result is

$$T_w = \frac{\dot{q}_g}{2\lambda_w} \delta_w^2 + \frac{q''_{loss}}{\lambda_w} \delta_w + T'_w. \qquad (19)$$

The heat loss through the insulation to the surroundings is evaluated by measuring the back surface temperature of the insulation and the ambient temperature. With these data a standard correlation can be used to estimate the heat loss. The back surface temperature of the insulation is measured by T-type thermocouples at five longitudinal locations along the insulation, and the average (arithmetic) insulation temperature T_{ins} is determined. The loss is then computed by the suggested correlation for natural convection from a vertical plate in air, as recommended by Holman [22].

Flow Rate Measurement The flow rate of the liquid film is measured by a variable-area flowmeter (M-type). All the flowmeters are calibrated by the static weighting procedure, as described by Mattingly [23], at several liquid temperatures to account for the property variations with

temperature. The accuracy of the flow rate measurement is believed to be within 0.009987 kg/min.

The gas flow rate is evaluated by integrating the velocity profile obtained by measuring the velocity at several positions in the cross section near $x = 10$ cm. The gas velocity is measured by a Pitot tube 67 cm long and 0.03 cm in diameter (Model PDA-24-F-22KL) and a high-precision manometer (Model P-600). The manometer allows calibration and measurement of differential, absolute, or gauge pressure within the range of 0–1 psi with 98.5% accuracy.

Uncertainty Analysis for Experimental Results

The purpose of performing an uncertainty analysis is to estimate the uncertainty levels in the experimentally determined Nusselt numbers. The procedures of the uncertainty analysis proposed by Kline and McClintock [24] and Moffat [25] were used. The uncertainties in the basic parameters and Nusselt number are presented in Table 1. It is noted that, except in the region near the leading edge ($x \leq 0.1$ m), the uncertainty in Nu_L is 3.8–14.3%.

RESULTS AND DISCUSSION

The problem under investigation is governed by six physical parameters: the inlet liquid temperature $T_{L,in}$, inlet liquid mass flow rate $\dot{m}_{L,in}$, free-stream water vapor concentration $W_{v,\infty}$, free-stream temperature $T_{G,\infty}$, free-stream velocity $u_{G,\infty}$, and imposed wall heat flux q_w''. In view of the large number of parameters, a fully parametric exploration is unrealistic. Rather, the parameters were varied systematically in order to examine the key trends in the results. Particular attention was paid to investigating the effects of q_w'', $\dot{m}_{L,in}$, $T_{L,in}$, and $u_{G,\infty}$ on the heat and mass transfer characteristics in the flow. The ranges of these parameters are as follows: q_w'', 1000–4000 w/m²; $\dot{m}_{L,in}$, 0.01–0.04 kg/(m s); $T_{L,in}$, 30–50°C; $u_{G,\infty}$, 0.5–4 m/s; with $T_{G,\infty}$ fixed at 30°C and $W_{v,\infty}$ at 0.013 (this corresponds to a relative humidity of 50%).

Table 1. Uncertainties in the Basic Parameters and Nusselt Numbers

Basic Parameter	Uncertainty
x distance, m	±0.0005
l, m	±0.0005
z, m	±0.0005
$T_{L,in}$, °C	±0.15
T_w, °C	±0.15
$T_w - T_{L,in}$, °C	±0.21
I, A	±1%
V, V	±1%
$\dot{Q}_{tot}$, W	±1.4%
q_w'', W/m²	±3.5%
λ_L, W/(m²°C)	±1%
ν_L, m²/s	±1%

Calculated uncertainty in Nu_L 3.9–14.3%

Shown in Fig. 3 are the predicted temperature distributions in the liquid film and gas stream for cases with $T_{L,in} = 30°C$, $u_{G,\infty} = 2$ m/s, and $\dot{m}_{L,in} = 0.02$ kg/(m s) under various heating conditions. The inserted plots in these figures provide a close look at the heat transfer process near the interface. The dashed line in each insert marks the location of the liquid/gas interface. Comparison of the corresponding curves in Figs. 3a and 3b at the same x indicates that an increase in q_w'' results in a higher temperature rise in the liquid film and gas stream. The concentration distributions of the water vapor in the gas stream, given in Fig. 4, show that the water vapor in the interface region increases in the flow direction and more water vapor exists in the gas stream when q_w'' is higher. The trend is similar to the temperature development in Fig. 3 since thermodynamic equilibrium was assumed at the interface, Eq. (10).

Presented in Figs. 5–7 are the measured and predicted wall temperature distributions along the plate for various cases. First, it is observed that the measured and predicted
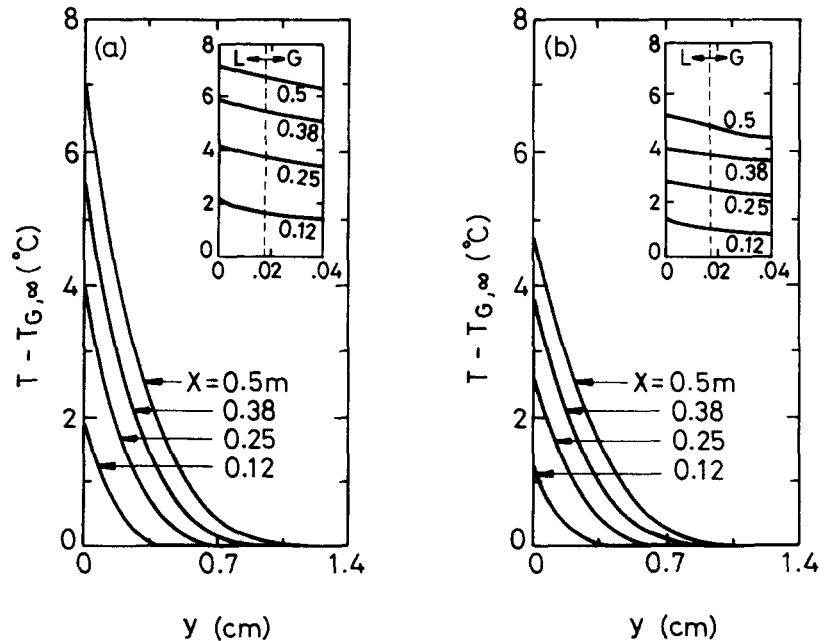

Figure 3. Developments of temperature profiles for $\dot{m}_{L,in} = 0.02$ kg/(m s), $T_{L,in} = 30°C$, $u_{G,\infty} = 2$ m/s, and (a) $q'' = 2000$ w/m², (b) $q_w'' = 1500$ w/m².
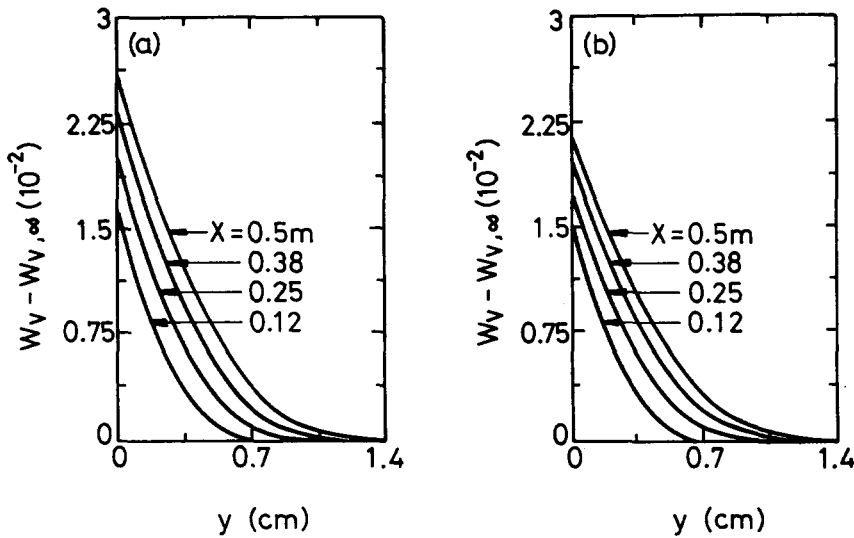
Figure 4. Developments of mass fraction profiles of water vapor for $\dot{m}_{L,in} = 0.02$ kg/(m s), $T_{L,in} = 30°C$, $u_{G,\infty} = 2$ m/s, and (a) $q_w'' = 2000$ w/m^2; (b) $q_w'' = 1500$ w/m^2.

wall temperatures are in good agreement, which lends strong support to the theoretical model employed in the computation. The effects of the imposed wall heat flux are illustrated in Fig. 5. As expected, a larger temperature rise results for a system with a larger input heat flux. Careful scrutiny of the curves in this figure reveals that the wall temperature rise per unit heat flux input, $\Delta T_w/q_w''$, is higher for the case with a larger q_w''. This suggests that for a system with a larger q_w'', a smaller part of the input heat transfers across the liquid film to cause the film vaporization and a larger part of the input heat goes to heat up the liquid film.

The effects of the inlet liquid temperature on the wall temperature distributions are shown in Fig. 6. The results indicate that the temperature rise is less for the case with higher inlet liquid temperature at the same heating condition. This is readily understood by realizing that the film vaporization is stronger when the liquid temperature is

higher, which in turn causes a larger amount of energy to be transported to the interface to sustain the required latent heat of vaporization ($m_{v,i}'' h_{LG}$). Thus, the fraction of the heat input to the system through the plate that goes to heat up the liquid film decreases with an increase in the inlet liquid temperature, and consequently the temperature rise of the liquid film is smaller. It is interesting to note that for $T_{L,in} = 50°C$ the wall temperature decreases in the upstream region although the plate is being heated. This is due to the fact that the energy required to sustain the latent heat of film vaporization is much larger than the heat input from the plate in this region, as can be clearly seen later in Fig. 8. To maintain energy conservation, the energy required for film vaporization is also supplied by the liquid film through the loss of sensible heat, and thus the liquid film is cooled. The wall tempera-
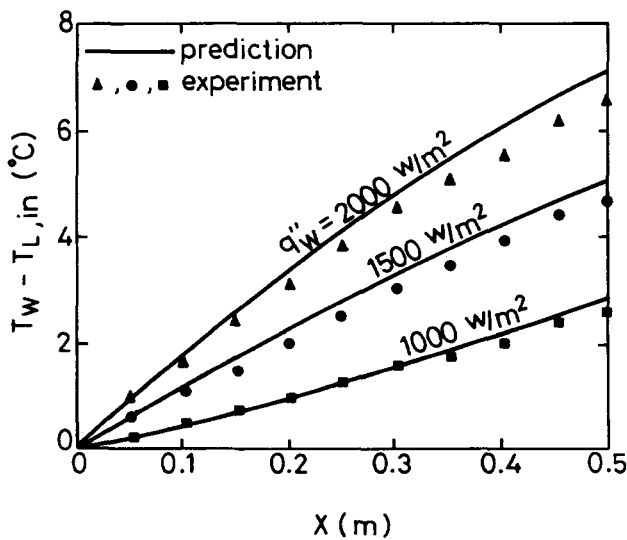

Figure 5. Effects of wall heat flux on the local wall temperature distributions for $m_{L,in} = 0.02$ kg/(m s), $T_{L,in} = 30°C$, and $u_{G,\infty} = 2$ m/s.
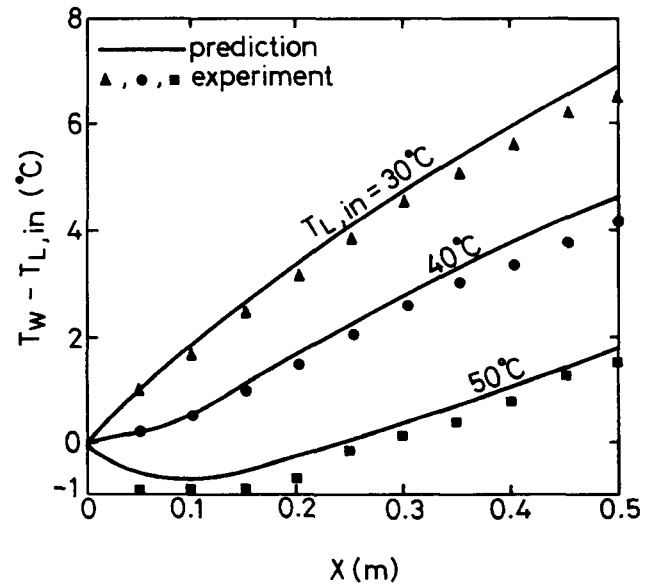

Figure 6. Effects of inlet liquid temperature on the local wall temperature distributions for $q_w'' = 2000$ w/m^2, $\dot{m}_{L,in} = 0.02$ kg/(m s), and $u_{G,\infty} = 2$ m/s.
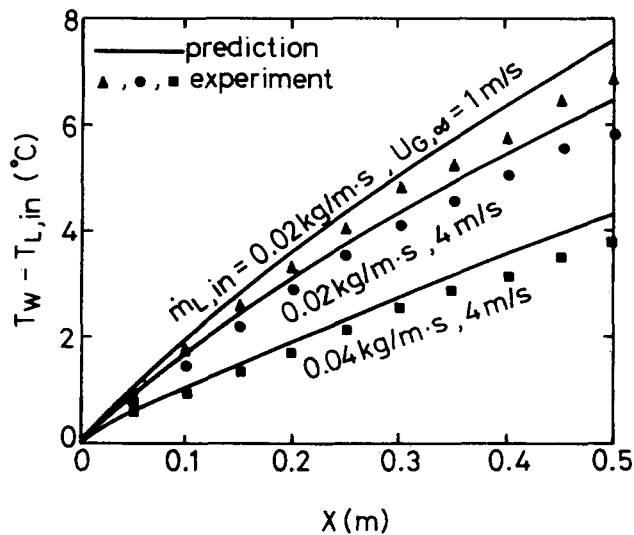
Figure 7. Effects of inlet liquid mass flow rate and free-stream velocity on the local wall temperature distributions for $q_w'' = 2000$ w/m^2 and $T_{L,in} = 30°C$.

Figure 8. Local interface heat flux distributions for $q_w'' = 2000$ w/m^2, $\dot{m}_{L,in} = 0.02$ kg/(m s), and $u_{G,\infty} = 2$ m/s. (a) Latent heat; (b) sensible heat; (c) overall.

ture distributions given in Fig. 7 show that a smaller temperature rise is encountered for a system with a larger $\dot{m}_{L,in}$ at a constant q_w''. Also shown in Fig. 7 are the effects of the gas stream velocity. A lower T_w is noted at higher $u_{G,\infty}$. This reflects the fact that the cooling of the liquid film is more effective for a system with a higher $u_{G,\infty}$.

Physically, the heat input to the system goes to heat the liquid film and transports across the film to cause film vaporization and an increase in the gas temperature. To improve our understanding of the interface heat transfer characteristics, Figs. 8a–c have been prepared to show the predicted distributions of the interface latent heat flux absorbed by the film vaporization $(m_{v,i}'' h_{LG})$, interface sensible heat flux on the gas side $(-\lambda_G \, \partial T_G/\partial y|_i)$, and total interface heat flux (latent heat + sensible heat). First, by comparing the ordinate scales of Figs. 8a and 8b, it is apparent that $q_{e,i}''$ is much larger than $q_{s,i}''$. For a fixed $T_{L,in}$, $q_{e,i}''$ is about 10 times larger than $q_{s,i}''$. This indicates that the energy transfer across the film is mostly absorbed by the process of film vaporization. Also noted in Fig. 8a is that a higher $T_{L,in}$ results in a larger $q_{e,i}''$ because of the greater film vaporization associated with it. A similar trend is noted in the sensible heat transfer at the interface (Fig. 8b), which is simply due to the larger temperature difference $T_{L,i} - T_{G,\infty}$ for the system with higher $T_{L,in}$. For the special case of $T_{L,in} = 30°C$, the liquid film has the same temperature as the gas stream at the leading edge $(x = 0)$, and hence no sensible heat exchange occurs between the liquid film and the gas stream. Thereafter, the continuous rise of the liquid temperature causes the increase in $q_{s,i}''$ in the flow direction. This trend is different from the cases with $T_{L,in} = 40$ and $50°C$.

The distributions of the total heat flux at the interface, given in Fig. 8c, show that at a higher $T_{L,in}$ (50°C) the heat input to the system mostly transfers across the liquid film and only about 10% of the heat input goes to heat up the liquid film. It is important to point out that for the curves with $T_{L,in} = 40$ and $50°C$, q_i''/q_w'' exceeds unity in
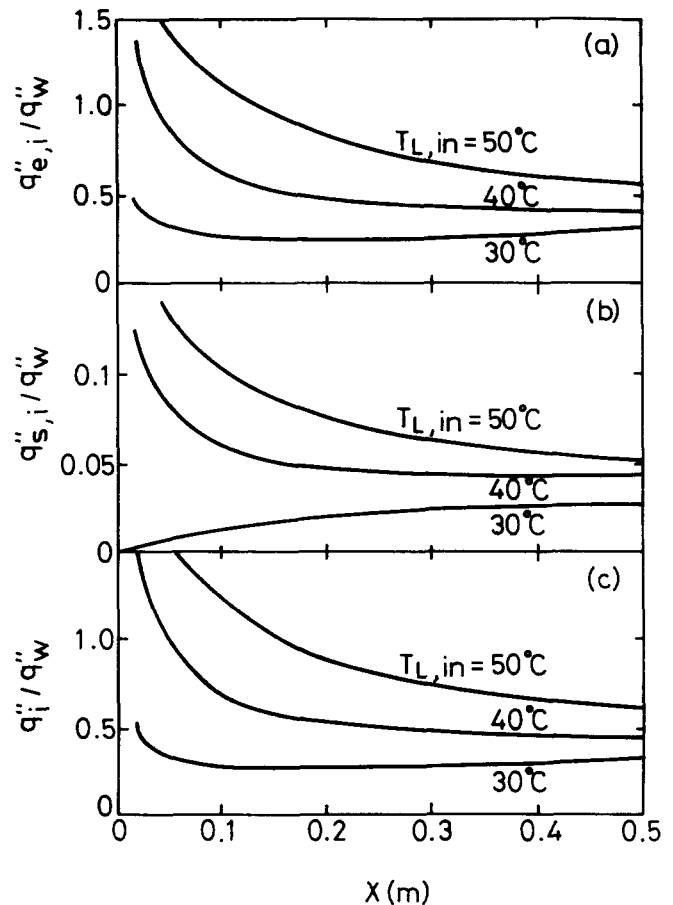
the upstream region. This is due to the intensive film vaporization in this region. Thus, the energy required to provide the vaporization is greater than the imposed wall heat flux.

Attention is now turned to investigating the influences of the wall heat flux on the local Nusselt number variations for heat transfer from the wall to the liquid film. In Fig. 9 we note that for a given q_w'' the local Nusselt number decreases monotonically in the flow direction due to the continuous increase in the wall temperature with x. In addition, a higher Nu_L is associated with a lower wall heat flux. This is consistent with the previous statement on Fig. 3b that the wall temperature rise per unit heat input is higher for a higher q_w''. Also, it is noted that good agreement exists between the measured and predicted Nu_L values.

It is observed from Fig. 10 that Nu_L is higher for a system with a higher $T_{L,in}$ because the temperature difference $T_w - T_{L,in}$ is smaller when the liquid inlet temperature is higher. Figure 11 presents the effects of $\dot{m}_{L,in}$ and $u_{G,\infty}$ on the distributions of Nu_L. Higher Nu_L values are found for larger $\dot{m}_{L,in}$ and $u_{G,\infty}$.

In practical applications, empirical correlations for the distributions of the local Nusselt number Nu_L are of great
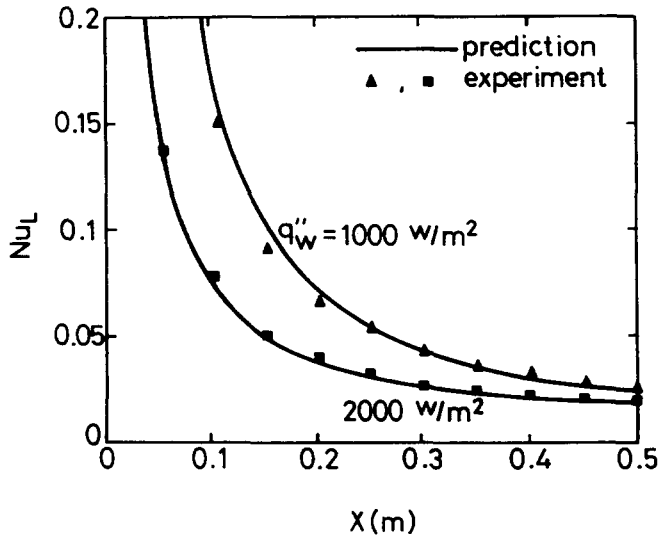
Figure 9. Effects of wall heat flux on the local Nusselt number distributions for $m_{L,in} = 0.02$ kg/(m s), $T_{L,in} = 30°C$, and $u_{G,\infty} = 2$ m/s.

value. To correlate the results from this study, a nondimensional parameter is introduced,

$$S = \frac{\rho_G Dh_{LG}(W_{v,r} - W_{v,\infty})}{q''_w x}. \tag{20}$$

It is noted that S signifies the importance of latent heat transfer in connection with the film vaporization. In addition, the Reynolds number for the gas stream is specifically defined as

$$Re_G = \frac{u_{G,\infty}(\nu_L^2/g)^{1/3}}{\nu_G}. \tag{21}$$

Our recommended correlation of Nu_L is
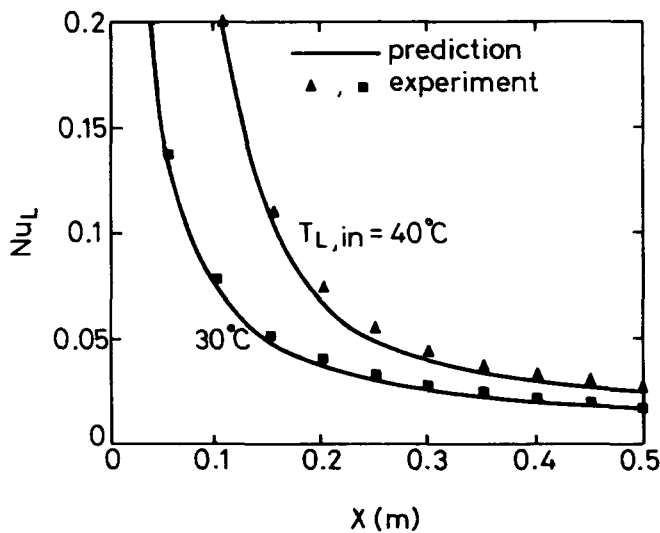
$$Nu_L = 0.76 S^{1.1} Re_L^{0.7} Re_G^{0.14}, \tag{22}$$

Figure 10. Effects of inlet liquid temperature on the local Nusselt number distributions for $q''_w = 2000$ w/m^2, $m_{L,in} = 0.02$ kg/(m s), and $u_{G,\infty} = 2$ m/s.
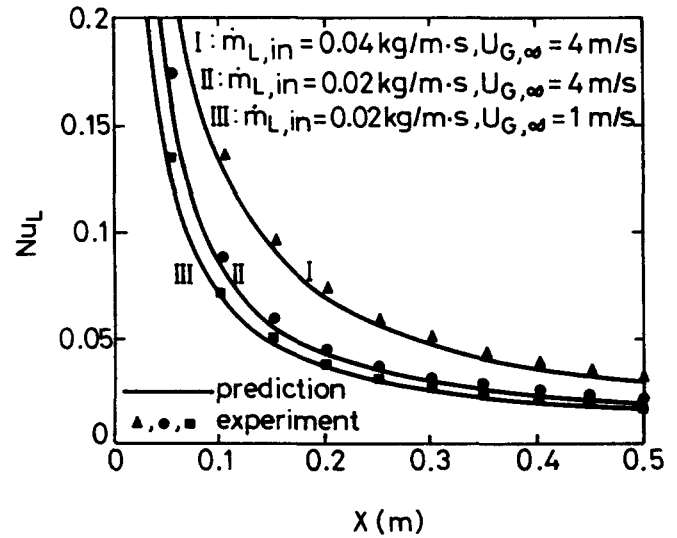

Figure 11. Effects of inlet liquid mass flow rate and free-stream velocity on the local Nusselt number distributions for $q''_w = 2000$ w/m^2, $T_{L,in} = 30°C$.

which is based on the experimental data for $3.7 \times 10^{-4} < S < 3.7 \times 10^{-2}$, $100 < Re_L < 250$, and $0.93 < Re_G < 8.52$.

PRACTICAL SIGNIFICANCE

In engineering applications, the temperature variations of the heated plate wetted by a thin evaporating liquid film are of interest to thermal designers. To estimate the wall temperature, a one-dimensional analytic method is usually used. In this method, the coupling one-dimensional conservation equations for the liquid film and gas stream must be solved together. Prior to solving the coupling equations, the coefficients for heat transfer from the heated wall to the liquid film and from the liquid/film interface to the liquid/gas interface and the coefficients for heat and mass transfer from the interface to the gas stream must be provided empirically. These data can be readily evaluated from the present study. Moreover, from this study a simple method is proposed here for estimating the wall temperature. For a given flow and thermal condition, T_w is estimated as follows.

1. Assume a wall temperature T_w.
2. Evaluate the saturated mass fraction of water vapor at T_w and P_0.
3. Calculate the parameter S.
4. Calculate the Nusselt number Nu_L from Eq. (22), and find the heat transfer coefficient h_L from Eq. (15).
5. Find the wall temperature T_w from Eq. (14).
6. Check whether the error between the assumed wall temperature and that obtained from step 5 is small enough. If not, repeat steps 1–6. If yes, the solution converges.

CONCLUSION

A combined numerical and experimental analysis has been carried out to explore the heat and mass transfer charac-

teristics in a laminar gas stream flowing over an evaporating liquid film falling along a vertical plate subjected to a constant wall heat flux. The influences of thermal condition, inlet liquid mass flow rate, and gas stream velocity on the heat and mass transfer in the liquid film and the gas stream are investigated in detail. The predicted wall temperature and Nusselt number distributions compared favorably with the measured data. What follows is a brief summary of the major results.

1. Heat transfer between the liquid film and gas stream is dominated by the transport of latent heat in conjunction with the evaporation of the liquid film.
2. The evaporative latent heat transfer depends largely on the inlet liquid temperature $T_{L,in}$ and the wall heat flux q_w''.
3. In the ranges of the experimental conditions, the Nusselt number for heat transfer from the heated wall to the liquid film was correlated by a simple equation.

It has been realized during the course of the study that when $T_{L,in}$ is much higher than $T_{G,\infty}$ or when the plate is subjected to a high wall heat flux, the upward combined buoyancy force may result in flow reversal of the gas stream in certain parts of the flow field for small values of $u_{G,\infty}$. In this situation, a more complicated elliptic flow analysis must be performed.

NOMENCLATURE

C_p specific heat, kJ/(kg K)
D mass diffusivity, m²/s
g gravitational acceleration, m/s²
h_L heat transfer coefficient [$= q_w''/(T_w - T_{L,in})$], W/(m² K)
h_{LG} latent heat of vaporization, kJ/kg
I electric current, A
l length of heated plate, m
M molecular weight, kg/(kg mole)
$\dot{m}_L$ mass flow rate of liquid water per unit heated plate width, kg/(m s)
$m_{v,i}''$ interface mass flux of water vapor, Eq. (12), kg/(m² s)
Nu_L Nusselt number $= h_L(\nu_L^2/g)^{1/3}/\lambda_L$, dimensionless
P pressure, Pa
$\dot{Q}_{tot}$ total electrical dissipated heat rate in heated plate, W
$q_{e,i}''$ interface latent heat flux $= m_{v,i}'' h_{LG}$, W/m²
$\dot{q}_g$ heat generation per unit volume in heated plate, W/m³
q_i'' overall interface heat flux $= q_{e,i}'' + q_{s,i}''$, W/m²
q_{loss}'' heat flux through insulation to surroundings, W/m³
$q_{s,i}''$ interface sensible heat flux in gas side $= -(\lambda_G \, \partial T_G/\partial y)_{G,i}$, W/m²
q_w'' wall heat flux, W/m²
Re_G Reynolds number of gas stream $= u_{G,\infty}(\nu_L^2/g)^{1/3}/\nu_G$, dimensionless

Re_L Reynolds number of liquid film $= (4\dot{m}_L/\mu_L)$, dimensionless
S parameter $= \rho_G D h_{LG}(W_{v,r} - W_{v,\infty})$, W/m
T temperature, K
T_w' measured back surface temperature of heated plate, K
u longitudinal velocity, m/s
V Voltage drop across a heated plate, V
v transverse velocity, m/s
W_v mass fraction of water vapor, dimensionless
$W_{v,r}$ saturated mass fraction of water vapor at T_w and P_o, dimensionless
x, y longitudinal and transverse coordinates, m
$\Delta x, \Delta y$ longitudinal and transverse grid sizes, m
z plate width, m

Greek Symbols

δ_L liquid film thickness, m
δ_w plate wall thickness, m
λ conductivity, W/(m K)
μ dynamic viscosity, Pa · s
ν kinematic viscosity, m²/s
ρ density, kg/m³
ρ_e electrical resistivity, Ω m

Subscripts

a   of air
G   of gas stream
i   at interface
in   at inlet
j, k the jth longitudinal and kth transverse grid points
L   of liquid
v   of water vapor
w   of wall
∞ free-stream value

REFERENCES

1. Chun, K. R., and Seban, R. A., Heat Transfer to Evaporating Liquid Film, *J. Heat Transfer* **93**(3), 391–396, 1971.
2. Seban, R. A., and Faghri, A., Evaporation and Heating with Turbulent Falling Liquid Films, *J. Heat Transfer* **98**(2), 315–318, 1976.
3. Gill, W. N., Casal, E. D., and Zeh, D. W., Binary Diffusion and Heat Transfer in Laminar Free Convection Boundary Layers on a Vertical Plate, *Int. J. Heat Mass Transfer* **8**(8), 1135–1151, 1965.
4. Saville, D. A., and Churchill, S. W., Simultaneous Heat and Mass Transfer in Free Convection Boundary Layers, *AIChE J.* **16**(2), 268–273, 1970.
5. Bottemanne, F. A., Theoretical Solution of Simultaneous Heat and Mass Transfer by Free Convection About a Vertical Flat Plate, *Appl. Sci. Res.* **25**(1/2), 137–149, 1971.
6. Gebhart, B., and Pera, L., The Nature of Vertical Natural Convection Flows Resulting from the Combined Buoyancy Effects of Thermal and Mass Diffusion, *Int. J. Heat Mass Transfer* **14**(12), 2025–2050, 1971.
7. Chen, T. S., and Yuh, C. F., Combined Heat and Mass Transfer in Natural Convection on Inclined Surfaces, *Numer. Heat Transfer* **2**(2), 233–250, 1979.

8. Chang, C. J., Lin, T. F., and Yan, W. M., Natural Convection Flows in a Vertical Open Tube Resulting from Combined Buoyancy Effects of Thermal and Mass Diffusion, *Int. J. Heat Mass Transfer* 29(10), 1543–1552, 1986.

9. Chandra, V., and Savery, C. W., Forced Convective Heat and Mass Transfer from a Falling Film to a Laminar External Boundary Layer, *Int. J. Heat Mass Transfer* 17(12), 1549–1557, 1974.

10. Chandra, V., Mass, Momentum and Heat Transfer from a Falling Film to a Countercurrent Air Stream, Ph.D. thesis, Drexel Univ., Philadelphia, PA, 1975.

11. Schroppel, J., and Thiele, F., On the Calculation of Momentum, Heat and Mass Transfer in Laminar and Turbulent Boundary Layer Flows Along a Vaporizing Liquid Film, *Numer. Heat Transfer* 6(4), 475–496, 1983.

12. Chow, L. C., and Chung, J. N., Evaporation of Water into a Laminar Stream of Air and Superheated Steam, *Int. J. Heat Mass Transfer* 26(3), 373–380, 1983.

13. Chow, L. C., and Chung, J. N., Water Evaporation into a Turbulent Stream of Air, Humid Air or Superheated Steam, 21st ASME/AICHE Natl. Heat Transfer Conf., Seattle, WA, ASME Paper 83-HT-2, 1983.

14. Haji, M., and Chow, L. C., Experimental Measurement of Water Evaporation Rates into Air and Superheated Steam, *J. Heat Transfer* 110(1), 237–242, 1988.

15. Shembharkar, T. R., and Pai, B. R., Prediction of Film Cooling with a Liquid Coolant, *Int. J. Heat Mass Transfer* 29(6), 899–908, 1986.

16. Baumann, W. W., and Thiele, F., Heat and Mass Transfer in Two-Component Film Evaporation in a Vertical Tube, 8th Int. Heat Transfer Conf., Vol. 4, pp. 1843–1848, 1986.

17. Bird, R. B., Stewart, W. E., and Lightfoot, E. N., *Transport Phenomena*, Wiley, New York, 1960.

18. Yano, T., and Uchida, H., Thermophysical Properties of Fluids, *JSME Data Book*, JSME, Tokyo, 1983.

19. Fuji, T., Kato, Y., and Mihara, K., Expressions of Transport and Thermodynamic Properties of Air, Steam and Water, Sei San Ka Gaku Ken Kyu Jo, Report No. 66, Kyu Shu Univ., Kyu Shu, Japan, 1977.

20. Anderson, D. A., Tannehill, J. C., and Pletcher, R. H., *Computational Fluid Mechanics and Heat Transfer*, McGraw-Hill, New York, 1984.

21. Szewczyk, A. A., Combined Forced and Free-Convection Laminar Flow, *J. Heat Transfer* 86(4), 501–507, 1964.

22. Holman, J. P., *Heat Transfer*, 5th ed., McGraw-Hill, New York, 1981.

23. Mattingly, G. E., Volume Flow Measurements, in *Fluid Mechanics Measurements*, R. J. Goldstein, Ed., Chap. 6, Hemisphere, Washington, DC, 1983.

24. Kline, S. J., and McClintock, F. A., Describing Uncertainties in Single-Sample Experiments, *Mech. Eng.* 75, 3–8, 1953.

25. Moffat, R. J., Contributions to the Theory of Single-Sample Uncertainty Analysis, *J. Fluid Eng.* 104(2), 250–260, 1982.